Comparative Bioinformatics and Experimental Analysis of the Intergenic Regulatory Regions of Bacillus cereus hbl and nhe Enterotoxin Operons and the Impact of CodY on Virulence Heterogeneity

Boehm, Maria-Elisabeth; Krey, Viktoria M.; Jessberger, Nadja; Frenzel, Elrike; Scherer, Siegfried

Published in:
Frontiers in Microbiology

DOI:
10.3389/fmicb.2016.00768

Publication date:
2016

Journal of Medicinal Chemistry

Article

pubs.acs.org/jmc

Probing the Anticancer Action of Oridonin with Fluorescent Analogues: Visualizing Subcellular Localization to Mitochondria

Shengtao Xu,[†,△] Shanshan Luo,[‡,△] Hong Yao,[†] Hao Cai,[†] Xiaoming Miao,[§,#] Fang Wu,[*,∥] Dong-Hua Yang,[⊥] Xiaoming Wu,[†] Weijia Xie,[†] Hequan Yao,[†] Zhe-Sheng Chen,[⊥] and Jinyi Xu[*,†]

[†]State Key Laboratory of Natural Medicines and Department of Medicinal Chemistry, China Pharmaceutical University, 24 Tong Jia Xiang, Nanjing 210009, P. R. China

[‡]Department of Pharmacology, School of Pharmacy, Fudan University, Shanghai 201203, P. R. China

[§]State Key Laboratory of Medicinal Chemical Biology and College of Pharmacy, Nankai University, Tianjin 300071, P. R. China

[∥]Key Laboratory of Systems Biomedicine (Ministry of Education), Shanghai Center for Systems Biomedicine, Shanghai Jiao Tong University, Shanghai 200240, P. R. China

[⊥]College of Pharmacy and Health Sciences, St. John's University, 8000 Utopia Parkway, Queens, New York, New York 11439, United States

Supporting Information

ABSTRACT: Oridonin (**1**) is a complex *ent*-kaurane diterpenoid exhibiting remarkable antitumor activity. However, the detailed mechanism or cellular target that underlies this activity has not yet been identified. Herein, we report an efficient approach for exploring the anticancer mechanism of oridonin through development of the potent fluorescent analogues. A series of novel fluorescent oridonin probes linked with coumarin moieties were designed, synthesized, and characterized. Fluorescence microscopy and confocal imaging studies suggested that fluorescent oridonin probe **17d** was rapidly taken up into tumor cells and the mitochondrion was the main site of its accumulation. Moreover, we confirmed that cytochrome c played an important role in oridonin induced mitochondrion-mediated apoptosis and α,β-unsaturated ketone is the active moiety of oridonin, which is crucial to its uptake, localization, and cytotoxicity. Our results provide new insights on the molecular mechanism of oridonin and would be useful for its further development into an antitumor agent.

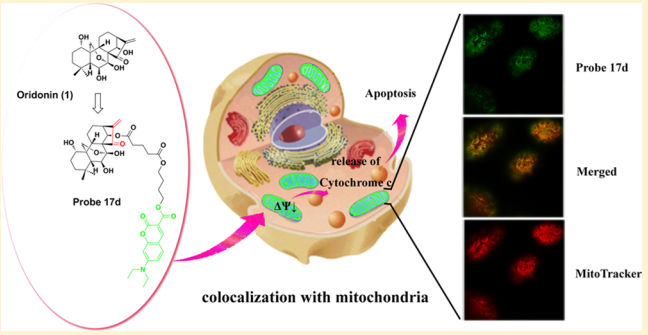

INTRODUCTION

In the last few decades, natural products have remained an important source for anticancer drug discovery.[1,2] *Isodon* species are widely distributed plants, and more than 600 diterpenoids have been isolated from this species over the past 30 years.[3] Many *Isodon* diterpenoids have been tested in laboratory assays against tumor cells, and a few compounds have shown potent antiproliferative activity with low toxicity, especially those with an *ent*-kaurane skeleton such as oridonin (**1**),[4] eriocalyxin B (**2**),[5] longikaurin A (**3**),[6] nodosin (**4**),[7] and so on (Figure 1, **1**−**5**).[8] The unique skeletons as well as their potent antitumor activities have made these diterpenoids promising candidates as anticancer agents.[9]

Oridonin (**1**) has been attracting increasing attention in recent years by cancer biologists due to its remarkable antitumor activity.[10−13] Evidence has suggested that oridonin exerts extensive antineoplastic activities against various human cancer cells while exhibiting relatively low toxicity.[14] This unique and safe anticancer pharmacological profile of oridonin stimulated interest in the research of its mechanism of anticancer action and structural modifications. Previous studies have revealed that oridonin could induce cell cycle arrest, apoptosis, and autophagy[15] by regulating a series of transcriptional factors.[16,17] For instance, Bu et al. reported that oridonin could induce apoptosis via p53- and caspase-dependent induction of p38 MAPK in SW1990 pancreatic cancer cells.[18] Xu et al. revealed that in pancreatic cancer BxPC-3 cells, oridonin could up-regulate p53 and down-regulate CDK1, which led to cell cycle arrest in the G2/M phase.[19] Additionally, Tommasi employed a mass spectrometry-based chemical proteomics approach to uncover target proteins of oridonin and suggested HSP70 1A as a potential target for oridonin in Jurkat cells.[20]

In spite of the preclinical success of oridonin, its detailed anticancer mechanism, mode of action, and intracellular target remain elusive. Further development of oridonin for cancer therapy was hampered largely due to these weaknesses. Therefore, expanding the scarce knowledge of the antineoplastic molecular mechanism and potential binding proteins of

Received: March 18, 2016
Published: April 18, 2016

DOI: 10.1021/acs.jmedchem.6b00408
J. Med. Chem. 2016, 59, 5022−5034

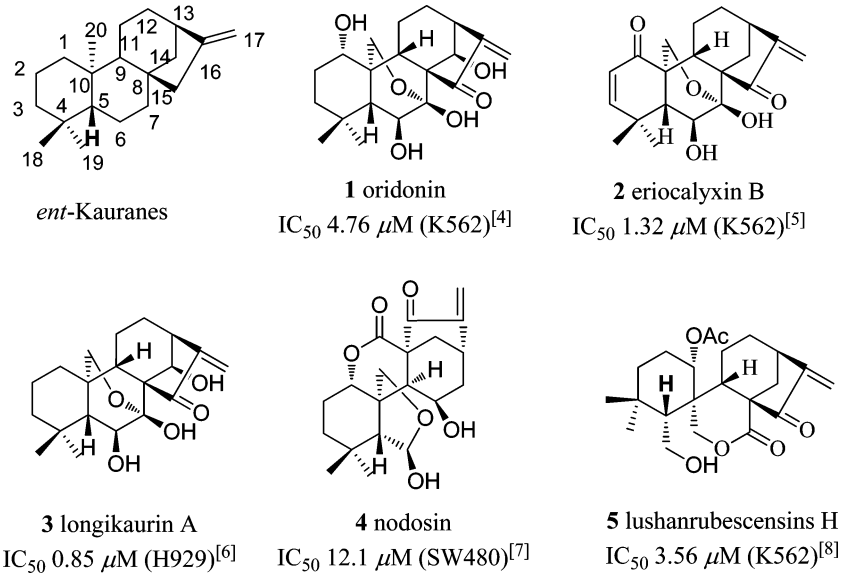

Figure 1. Structures of typical natural *ent*-kaurane diterpenoids.

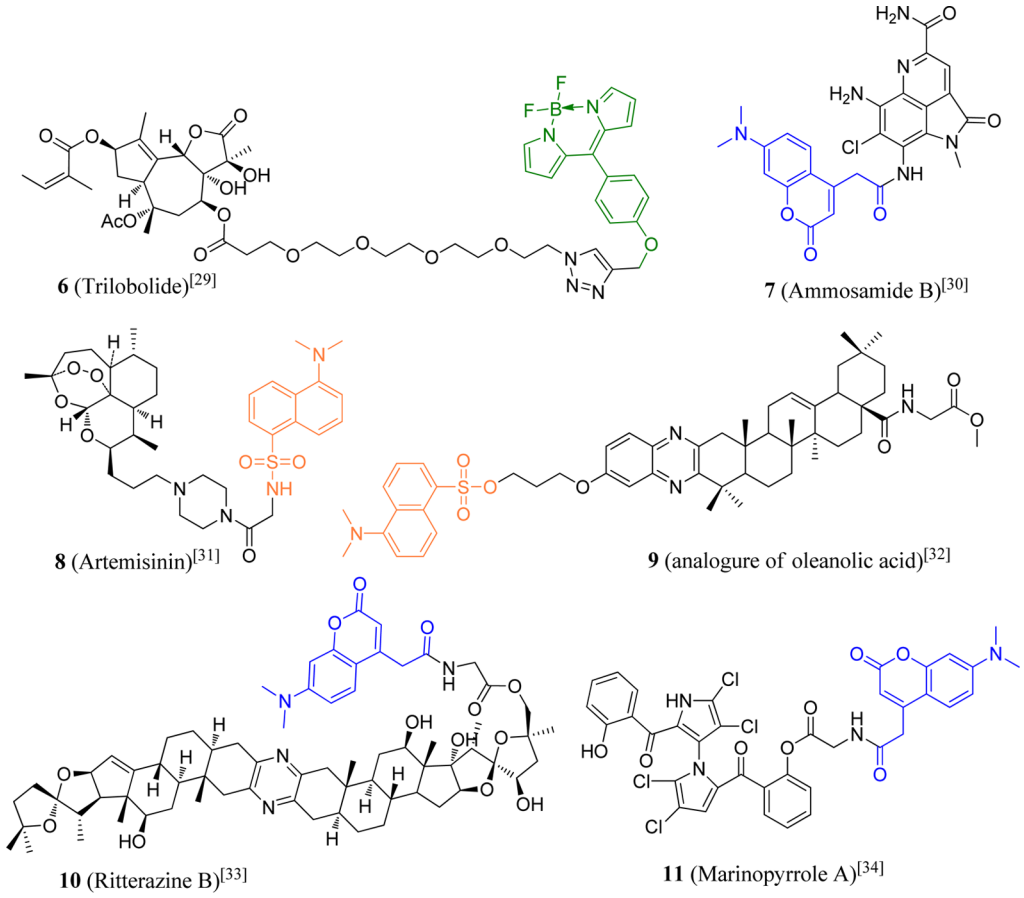

Figure 2. Structures of reported fluorescent natural product probes.

oridonin for further rational new drug design is an unmet need. More importantly, a systematic approach to target elucidation would facilitate both the introduction of new drugs into clinical practice and undesired targets identified.[21] However, discovering these functional targets and clarifying the mechanisms of bioactive natural products have proven to be especially perplexing due to the structural complexity of natural products, low abundance of targets in vivo, and limitations of bioanalytical methods.[22]

Despite these obstacles, a number of remarkable strategies have been developed to tackle these challenges.[23,24] Fluorescence imaging is such a strategy that has been widely used to visualize cell events and associated phenotypes at many levels, from molecules to complete organisms.[25,26] In recent years, natural products linked to fluorescent organic dyes for

DOI: 10.1021/acs.jmedchem.6b00408
J. Med. Chem. 2016, 59, 5022−5034

Scheme 1. Synthesis of Fluorescent Oridonin Probes 17a−e[a]

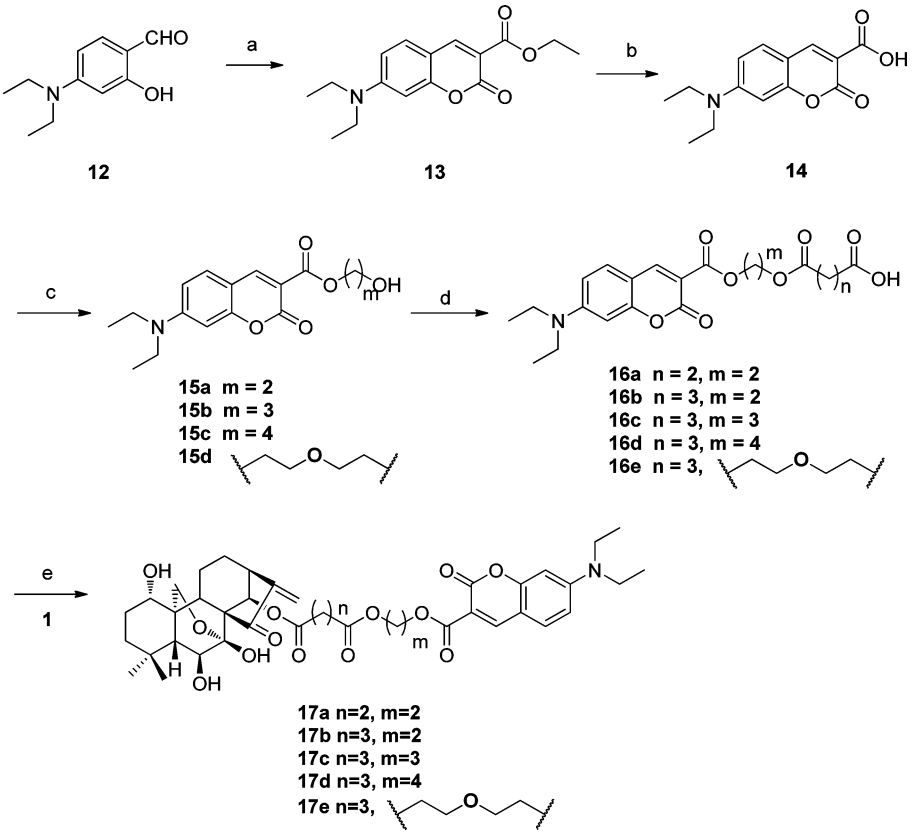

[a]Reagents and conditions: (a) ethylpropanedioate, piperidine, MeOH, reflux, overnight; (b) 10% NaOH, rt, 24 h; (c) corresponding diols, DMAP, EDCI, CH_2Cl_2, rt, 8−48 h; (d) glutaric anhydride or succinic anhydride, DMAP, CH_2Cl_2, rt, 48−72 h; (e) EDCI, DMAP, CH_2Cl_2, rt, 0.5−2 h.

Scheme 2. Synthesis of Fluorescent Oridonin Probes 24a−c[a]

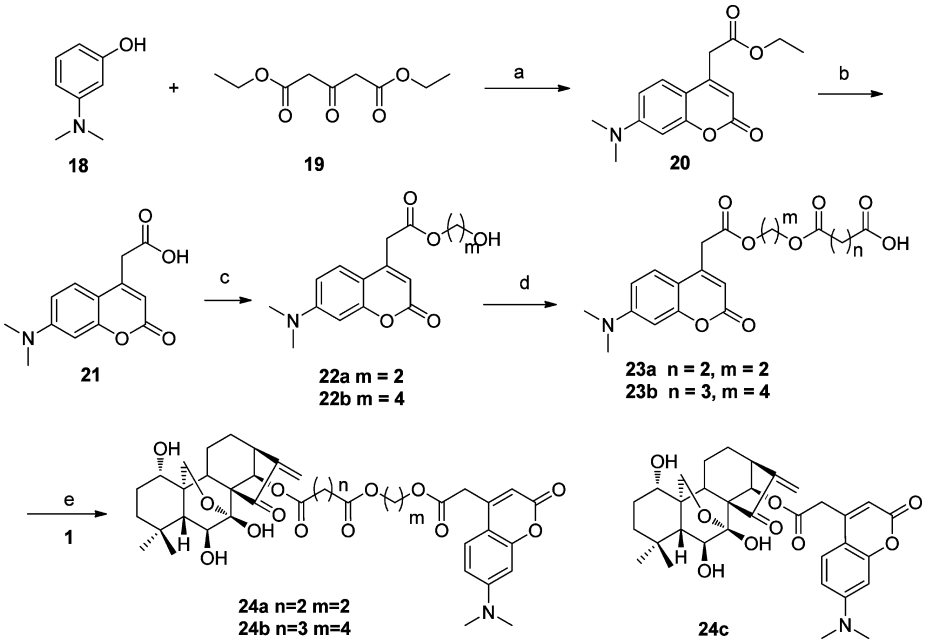

[a]Reagents and conditions: (a) MeOH, $ZnCl_2$, reflux, overnight; (b) 10% NaOH, rt, 24 h; (c) corresponding diols, DMAP, CH_2Cl_2, rt, 12−18 h; (d) glutaric anhydride or succinic anhydride, DMAP, CH_2Cl_2, rt, 48−72 h; (e) EDCI, DMAP, CH_2Cl_2, rt, 0.5−1 h.

fluorescence imaging has become a powerful tool to explore biological phenomena and provide insights into their mechanisms of action at many levels.[27,28] Reports for the use of bioactive fluorescent probes from natural products to investigate their modes of action and unveil the cellular processes including cellular uptake, localization, or specific

DOI: 10.1021/acs.jmedchem.6b00408
J. Med. Chem. 2016, 59, 5022−5034

Scheme 3. Synthesis of Oridonin Analogues 25, 26, and Fluorescent Oridonin Probe 27[a]

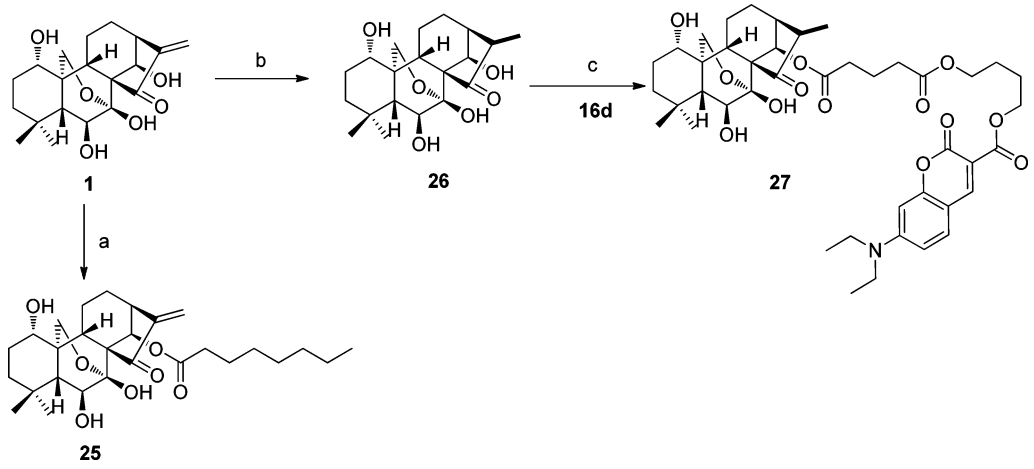

[a]Reagents and conditions: (a) *n*-caprylic acid, EDCI, DMAP, CH_2Cl_2, rt, 2 h; (b) 10% Pd/C, MeOH, rt, 1 h; (c) EDCI, DMAP, CH_2Cl_2, rt, 0.5 h.

interactions have already been developed (Figure 2, **6**–**11**).[29−34] In these cases, the application of fluorescent natural product probes has greatly contributed to the investigations of their modes of action and provided tools for visualization of their targets.

This perspective led us to develop fluorescent oridonin analogues that retain their cytotoxicity and yet has properties that facilitate its visualization within cells. We predicted that these novel fluorescent oridonin probes could provide insight into understand the subcellular localization, anticancer mechanism ,and structure−activity relationships (SARs) of oridonin and ultimately accelerate the development of oridonin as cancer therapeutics. Herein, we describe the design and synthesis of a series of novel fluorescent oridonin analogues and the application of these probes in revealing the anticancer action of oridonin.

RESULTS AND DISCUSSION

Design and Synthesis of Fluorescent Oridonin Probes. Fluorescent probes of natural products are typically generated by the attachment of a fluorophore to natural product via a proper linker, leaving the binding interactions unaltered. However, these interactions are often affect by linker type, length, and attachment point. Fortunately, our previous SARs analysis has revealed that the modification on 14-hydroxyl group of oridonin did not diminish its antiproliferative activity against a panel of human cancer cell lines.[35] With this in mind, fluorescent oridonin probes were designed and synthesized by connecting 14-hydroxyl group of oridonin with different coumarin moieties through linkers of various lengths. Specifically, highly fluorescent *N*,*N*-dialkyl-7-aminocoumarin derivatives (**14**, **21**, Schemes 1 and 2) were employed as fluorescent moieties because these fluorescent dyes has no toxicity and offer synthetic flexibility.[36,37]

As depicted in Scheme 1, fluorescent oridonin probes (**17a**−**e**) were synthesized from commercially available oridonin (**1**) in five steps. 7-(Diethylamino)coumarin-3-carboxylic acid (**14**) was first synthesized by the reaction of substituted salicylaldehyde (**12**) with ethylpropanedioate by using piperidine as the catalyst in methanol, followed by the hydrolysis of the corresponding coumarin ester (**13**) with 10% NaOH aqueous solution at room temperature in 56% overall yield over two steps. Because the length of the linkers may influence the hydrophobicity of the labeled molecules, diverse diols and anhydride handles were employed to further extend the variability of linker's length. For example, compound **15c** was obtained by the treatment of **14** with 1,4-butanediol (10 equiv) in the presence of DMAP and EDCI, followed by flash column chromatography purification in 85% yield. Then compound **15c** was treated with glutaric anhydride at room temperature to give the acid **16d**, which was further coupled with oridonin (**1**) in the presence of EDCI and DMAP in dry dichloromethane to deliver probe **17d** in 80% yield. Using similar methodology, reaction of oridonin with intermediates **16a**−**c** and **16e** gave other fluorescent probes **17a** (in 91% yield), **17b** (84%), **17c** (88%), and **17e** (72%), respectively. Interestingly, fluorescent side chains at C-14 position of oridonin can be highly regioselectively synthesized from oridonin without any protection, which was consistent with previous reports.[38] In addition, the structure of compound **17d** was unambiguously identified by 2D NMR experiments, whereby HMBC correlations were observed between the C14−H methine resonance (δ_H 5.88, 1H, s) of oridonin to ^{13}C resonances at δ_C 171.3 of the linker (please see Supporting Information).

7-(Dimethylamino)coumarin-4-acetic acid (**21**) was obtained in 29% overall yield by hydrolysis of the corresponding coumarin ester (**20**), which was formed by the reaction between 3-dimethylaminophenol (**18**) and diethyl-1,3-acetonedicarboxylate (**19**) in the presence of zinc chloride (Scheme 2). Fluorescent probe **24c** was prepared in 89% yield via ester condensation reaction between oridonin and compound **21** directly in the presence of EDCI and DMAP in dry dichloromethane. The other targeted fluorescent probes (**24a**−**b**) could be synthesized from intermediates **23a**−**b**, which were prepared using the same methods described above.

It has been widely accepted that the α,β-unsaturated ketone system in the D-ring of *ent*-kaurane diterpenoids is a key pharmacophore for their antiproliferactive activity, and destruction of this ketone system could counteract their anticancer effects. Thus, reductive oridonin (**26**) and its corresponding fluorescent probe (**27**) were prepared as negative controls as shown in Scheme 3. Reduction of the double bond between C-16 and C-17 of oridonin was accomplished by catalytic hydrogenation on 10% Pd/C in methanol at room temperature, then flash chromatography of

DOI: 10.1021/acs.jmedchem.6b00408
J. Med. Chem. 2016, 59, 5022−5034

the evaporated residue, eluting with dichloromethane/methanol (40:1) afforded compound **26** in 94% yield. The preparation of its fluorescent probe **27** was carried out by coupling compound **16d** to the C-14 position of **26** in 82% yield. On the other hand, compound **25** was employed as a positive control, which was synthesized in 80% yield through selective esterification of oridonin at 14-hydroxyl group with *n*-caprylic acid (Scheme 3).

Cytotoxicity. We investigated the antiproliferative activities of nine novel fluorescent oridonin probes including **17a−e**, **24a−c**, **27**, and two oridonin analogues **25** and **26** against human hepatocellular carcinoma Bel-7402 cells by using MTT assay. Oridonin (**1**) was also tested for comparison, and the data was summarized in Table 1. Oridonin and its 14-OH

Table 1. Growth Inhibitory Effects and Fluorescence Properties of Target and Reference Compounds

	inhibition rate (%)[a]			CH_2Cl_2[b]		
compd	100 μM (%)	10 μM (%)	1 μM (%)	λ_{exc} (nm)	λ_{em} (nm)	Stokes shift (nm)
1	94.6	94.8	37.9			
15a	9.5	3.7	0.7	443	465	22
17a	94.4	72.4	11.5	422	455	32
17b	94.6	85.0	4.9	425	458	33
17c	94.6	89.9	2.7	423	457	34
17d	93.8	94.0	88.6	420	454	34
17e	94.6	70.1	1.4	424	459	35
24a	93.3	46.4	1.1	381	468	87
24b	89.2	18.7	9.3	370	459	89
24c	92.4	94.5	13.6	377	457	80
25	94.7	92.7	57.5			
26	57.2	4.2	2.1			
27	37.2	3.7	1.8	432	461	29

[a]Growth inhibitory effects of compounds **1**, **17a−e**, **24a−c**, and **25−27** on human hepatocellular carcinoma Bel-7402 cells. MTT assays: Bel-7402 cells were treated with varying concentrations of indicated compounds for 72 h. Values are the mean of three independent experiments. [b]Fluorescence properties were evaluated in CH_2Cl_2 with compounds at a concentration of 1×10^{-6} M, λ_{exc}: maximum excitation, λ_{em}: maximum emission.

modified derivative **25** showed good cytotoxicity against Bel-7402 cells; however, analogue **26**, whose *α,β*-unsaturated ketone moiety was destructed, displayed poor antiproliferative activity. Almost all the fluorescent probes exhibited slightly lower antiproliferative activity compared with the parent oridonin, except probe **17d**. The probes containing 3-substituted coumarin (**17a−e**) maintained their cytostatic activity better than probes containing 4-substituted coumarin (**24a−c**). We also found that the length of spacer joining the coumarin skeleton and oridonin had an effect on the antiproliferative activities of the probes. Compound **17d**, with 11-atom spacer, expressed better inhibitory effect on growth than its analogues **17a−c** and **17e**. Although compound **24c** is more potent than **24a**, giving its short spacer which may interfere with the binding of natural product to its target and affect its mode of action, compound **24a** was more suitable for further studies.

On the basis of the above preliminary results, compounds **1**, **17d**, **24a**, **26**, and **27** were selected to further test their in vitro antiproliferative activities on three human cancer cell lines. As shown in Table 2, fluorescent probes **17d** and **24a** had

Table 2. IC_{50} Values of Oridonin (1), Its Synthetic Analogue (26), and Fluorescent Derivatives (17d, 24a, and 27) on Inhibiting Proliferation of Human Cancer Cells (μM)[a]

compd	HepG2	A549	Hela[b]
1	15.2 ± 1.0	10.4 ± 0.4	17.8 ± 0.9
17d	2.6 ± 0.1	5.1 ± 0.1	2.0 ± 0.1
24a	8.8 ± 0.6	11.2 ± 0.9	4.6 ± 0.2
26	70.6 ± 4.3	67.0 ± 7.1	52.7 ± 3.9
27	144.1 ± 9.5	78.0 ± 5.2	79.6 ± 6.3

[a]MTT assays: cells were incubated with indicated compounds for 72 h, (means ± SD, $n = 3$). [b]HepG2 (liver hepatocellular carcinoma cell), A549 (Human lung adenocarcinoma cell), Hela (human cervical cancer cell).

cytotoxicity comparable to, or even stronger than that of oridonin (**1**). However, compound **26** showed lower activity compared to that of oridonin, especially in A549 cell line (IC_{50}: 67.0 μM vs 10.4 μM), and its corresponding probe **27** also had no obvious activity as expected. These results suggested that *α,β*-unsaturated ketone moiety is crucial to the inhibitory activity of oridonin and its derivatives, and the coumarin moiety possesses low cytotoxicity.

Fluorescent Properties. As shown in Table 1, the fluorescent properties of target compounds including the excitation and emission of probes were evaluated in dichloromethane at a concentration of 1×10^{-6} M by using spectrofluorophotometer. All the probes exhibited significant differences between maximum excitation (λ_{exc}) and emission (λ_{em}) wavelength, namely Stokes shift. The probes bearing 3-substituted coumarin (**17a−e**, **27**) displayed fluorescence excitation peaks at about 425 nm and the emission wavelengths varied in the range of 454−459 nm, expressing a shift toward the UV region compared with probe **15a**. It was encouraging to see larger Stokes shift in these probes than **15a**, making them more appropriate for the imaging studies. We speculated that this might be attributed to the appended oridonin moiety. The probes bearing 4-substituted coumarin (**24a−c**) had larger Stokes shift (~80 nm) with λ_{exc} at ~380 nm and λ_{em} at ~460 nm. Preliminary studies on the fluorescent property showed that all these probes were suitable for imaging studies.

Uptake Profiles of Probes. The MTT assay showed that fluorescent probes **17d** and **24a** had significant antiproliferative activities comparable to that of oridonin. However, no obvious antiproliferative activities were observed on probes **15a** and **27**. Uptake profiles of these probes were detected to uncover the relationships between antiproliferative activities and uptake using fluorescence microscopy. As shown in Figure 3A, bright fluorescence staining inside the cells was observed when probes **17d** and **24a** were incubated at a concentration of 5 μM for 1 h in HepG2 cells. Then, cells stained with naked coumarin dye (**15a**) were used as a control to exclude the possibility that the uptake of the fluorescent oridonin probes was driven by coumarin dye itself. As shown in Figure 3Ac, no fluorescence could be detected from cells treated with 50 μM **15a**; as a matter of fact, even at a concentration of 100 μM, no obvious fluorescence could be observed after 1 h staining (Supporting Information, Figure S1). Unexpectedly, even at a concentration up to 20 μM, no fluorescence staining from probe **27** could be detected after 1 h incubation (Figure 3A-d). The lack of fluorescence from controls **15a** and **27** in live cells suggest that the uptake and localization was indeed due to the natural

DOI: 10.1021/acs.jmedchem.6b00408
J. Med. Chem. 2016, 59, 5022−5034

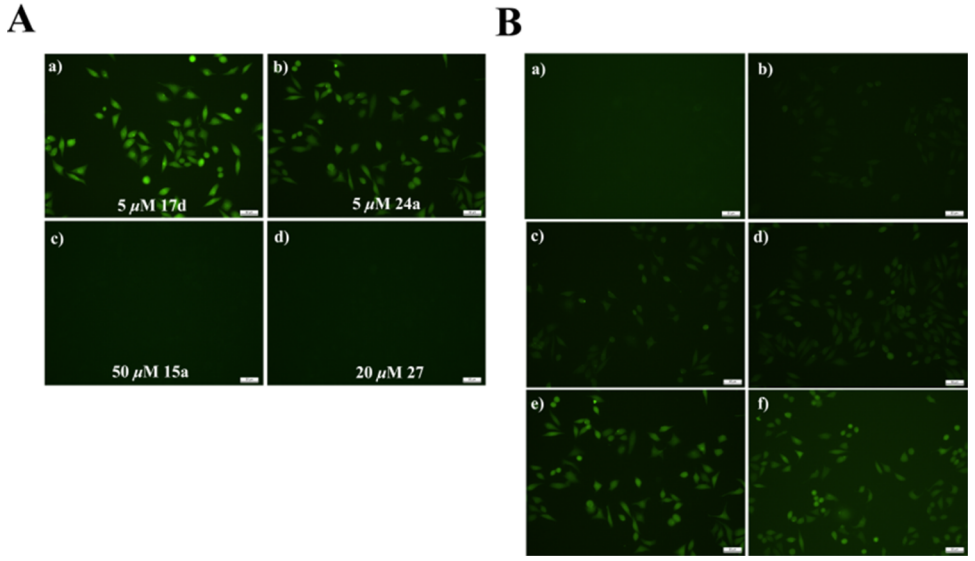

Figure 3. Uptake of probes in HepG2 cells. (A) Uptake of indicated probes in HepG2 cells: (a) 5 μM **17d** for 1 h, (b) 5 μM **24a** for 1 h, (c) 50 μM **15a** for 1 h, (d) 20 μM **27** for 1 h. (B) Time-course uptake of 1 μM probe **17d** in HepG2 cells, images were collected using fluorescence microscopy: (a) HepG2 cells were treated with **17d** for 0 min, (b) 5 min, (c) 10 min, (d) 15 min, (e) 30 min, (f) 1 h. Bars denote 50 μm.

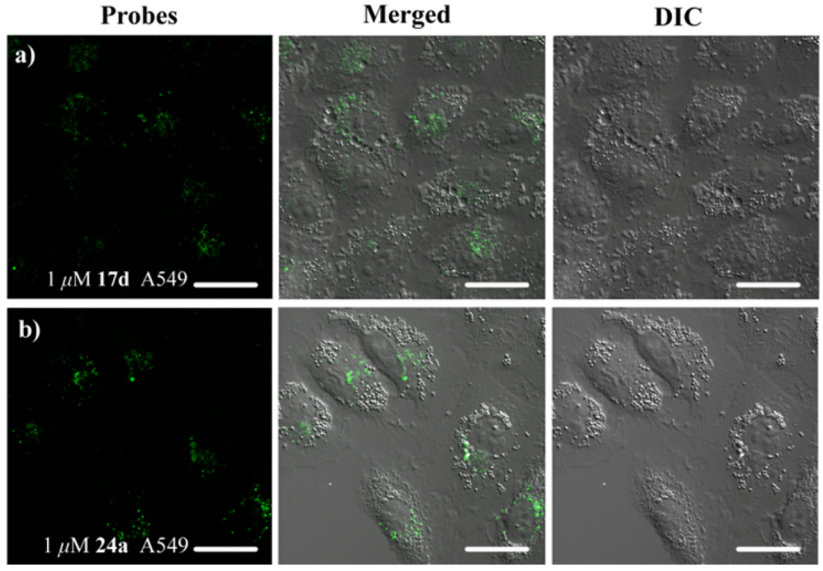

Figure 4. Live-cell imaging of probes. A549 cells were treated with 1 μM probe **17d** (a) or **24a** (b) for 12 h. Images were collected with excitation of probes at λ_{ex} = 405 nm and emission at λ_{em} = 460 nm, cells were imaged at 40× with an inverted confocal microscope (LSM710 NLO, Zeiss). DIC: differential interference contrast field. Bars denote 10 μm.

product's activity, and α,β-unsaturated ketone moiety is crucial to the uptake of oridonin.

In parallel, we performed time- and concentration-based uptake studies of probe **17d** in HepG2 cells. The minimum concentration of probe **17d** was optimized to 1 μM (data not shown), and the uptake of probe **17d** at this concentration was observed quickly as shown in Figure 3B. Notably, distinguishable fluorescence could be detected in HepG2 cells in as early as 5 min after incubation with probe **17d**, and the same phenomenon occurred when the A549 cells were incubated with **17d** (Supporting Information, Figure S2).

Intracellular Distribution of Probes 17d and 24a in Cancer Cells. To examine whether the types of linked coumarins would affect the uptake or localization of oridonin probes, we simultaneously investigated the difference between probes **17d** and **24a**, which were linked with different coumarin dyes. Both A549 and HepG2 cells were treated with 1 μM **17d** or **24a** for 12 h, washed with media, and imaged by a confocal laser scanning microscope. In HepG2 cells, probe **17d** appeared more effective than **24a** and stronger fluorescence signal could be detected from **17d** (Supporting Information, Figure S3), but no obvious difference could be observed in A549 cells (Figure 4) and the fluorescence signals of both **17d** and **24a** could be detected within the cytoplasm of cells presented as spots adjacent to the nuclear. Thus, the next subcellular localization studies were reasonably carried out in A549 cells.

Subcellular Localization Studies. To further detail the subcellular localization of fluorescent oridonin probe **17d** in A549 cells, we costained **17d**-treated cells with a panel of organelle-specific dyes. Fortunately, confocal microscopy of cells costained with MitoTracker Red (mitochondria specific dye) confirmed the localization of **17d** in mitochondria. In

DOI: 10.1021/acs.jmedchem.6b00408
J. Med. Chem. 2016, 59, 5022−5034

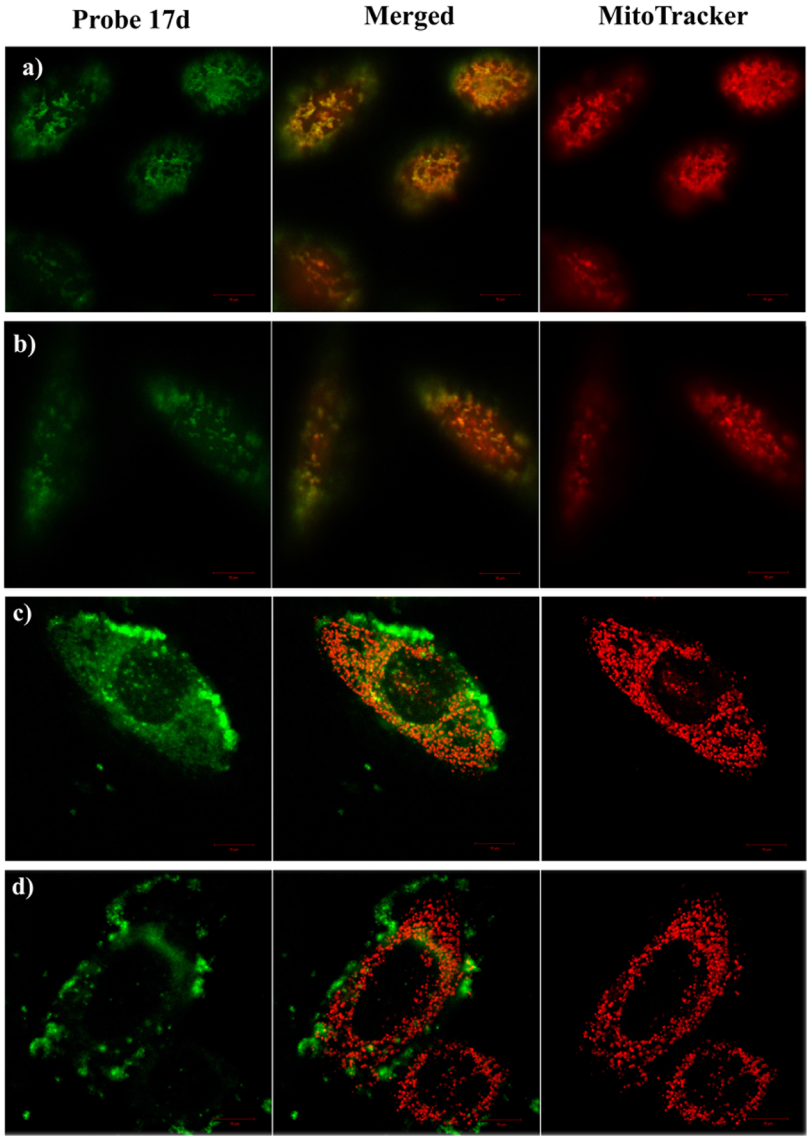

Figure 5. Time-course of co-localization of probe **17d** with MitoTracker (mitochondria specific dye) in A549 cells. Images were collected using confocal microscopy (LSM710 NLO, Zeiss, 60×). (a) A549 cells incubated with 1 μM **17d** for 1 h: right panel, cellular localization of **17d**; middle panel, overlay of two images; left panel, cellular localization of MitoTracker. A549 cells incubated with 1 μM **17d** for 3 h (b), for 12 h (c), for 24 h (d). Images were collected with excitation of probe **17d** at λ_{ex} = 405 nm and emission at λ_{em} = 460 nm, MitoTracker at λ_{ex} = 579 nm and emission at λ_{em} = 600 nm. Bars denote 10 μm.

particular, the overlap of red fluorescence from the red mitochondrial stain and the green fluorescence from probe **17d** provided compelling evidence in support of this conclusion (Figure 5a). Notably, in this localization study, probe **17d** was absorbed quickly after 1 h incubation and localized to mitochondria with a Pearson's coefficient value (*Rr*) of 0.979. However, the *Rr* value decreased to 0.843 when cells were treated with **17d** for 3 h, and only partial overlap of these two fluorescent probes could be observed at 12 h. After 24 h, no co-localization could be observed and the fluorescence became dispersed, which may be attributed to the cytotoxicity of probe.

Mitochondrial Membrane Potential Assay. The mitochondrion is an essential organelle that plays a crucial role in energy production; its dysfunction would induce irreversible cell apoptosis in a short time.[39] Inspired by the observations in which the fluorescent oridonin probe provided direct visual evidence for co-localization with mitochondria in A549 cells, we speculated that these fluorescent oridonin probes may reduce mitochondrial membrane integrity and thereby affect cell proliferation.[40] Thus, commercially available fluorescent probe JC-1 was used to measure the mitochondrial membrane potential (MMP). In healthy cells, JC-1 aggregates in the mitochondria and spontaneously forms complexes that fluoresce red. In apoptosis or necrotic cells, JC-1 exists in the monomeric form and stains the cytosol green. As shown in Figure 6a, treatment of A549 cells with 1 μM **17d** induced the dissipation of MMP in a time-dependent manner, as indicated by a decrease in red fluorescence emission and an increase in green fluorescence emission. The ratio of fluorescent intensity of red to green was determined and used as an indicator of cell healthy status. The ratio began to decrease after 12 h treatment of 1 μM **17d**, and after 48 h treatment, the ratio decrease dramatically from 1.496 to 0.312. However, no significant changes of MMP could be observed after the treatment of 20 μM **27** (Figure 6b).

DOI: 10.1021/acs.jmedchem.6b00408
J. Med. Chem. 2016, 59, 5022−5034

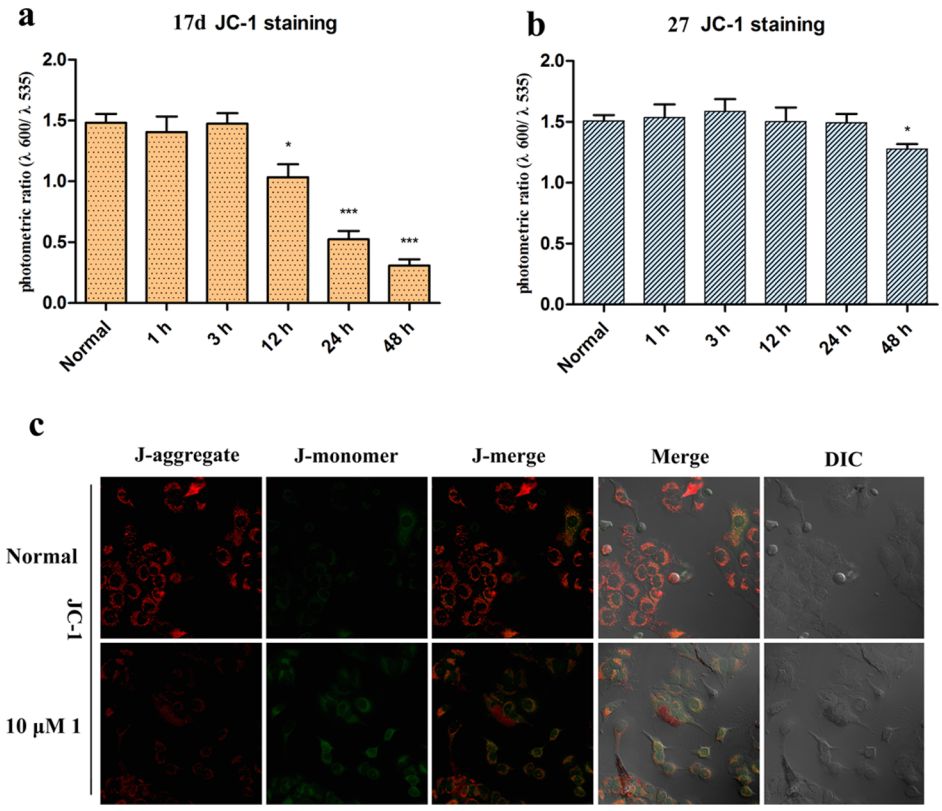

Figure 6. Compounds **17d** and **1** induced loss of mitochondrial membrane potential (MMP) in A549 cells analyzed by JC-1 fluorescence. (a) Independent experiments with 10000 cells per treatment condition reveal a decrease of photometric ratio of red to green fluorescence after **17d** treatment, and no significant change could be observed after **27** treatment (b). Data was represented as mean ± SD of three independent experiments, $*P < 0.05$, $**P < 0.01$, $***P < 0.001$. (c) Oridonin induced mitochondrial depolarization in A549 cells. After treatment with 10 μM **1** for 36 h, the fluorescence intensity changed significantly from red to green in treated cells. The upper panels represent the normal group, and lower panels depict the loss of MMP after the treatment of oridonin.

Previous investigations indicated that oridonin could induce apoptosis through several apoptotic pathways, especially mitochondria-dependent apoptosis.[41] Therefore, we detected the influence of oridonin on MMP using JC-1 probe. Briefly, A549 cells were first incubated with or without 10 μM oridonin for 36 h, then dyed with fluorescent JC-1. As shown in Figure 6c, oridonin treatment in A549 cells induced the dissipation of MMP, as indicated by a change of fluorescence intensity from red to green in treated cells. Collectively, these results suggested that mitochondrial pathway directly participated in apoptosis induced by oridonin.

Immunofluorescence Co-localization Analysis of Cytochrome c. Cytochrome c is widely believed to be localized uniquely in the mitochondrial intermembrane space under normal physiological conditions. The release of cytochrome c from mitochondria to the cytosol after the dissipation of MMP, where it activates the caspase family of proteases, is believed to be a primary trigger leading to the onset of apoptosis.[42] Thus, we detected the localization of cytochrome c in A549 cells after the treatment of oridonin with immunofluorescence co-localization analysis. As shown in Figure 7, in control groups, the green-stained cytochrome c by a fluorescently labeled secondary antibody were located in the mitochondria which were stained red by Mitotracker Red, resulting in a bright-orange fluorescence. However, when A549 cells were treated with 3 or 5 μM oridonin for 24 or 48 h, part of the orange fluorescence was quenched and green color appeared outside, indicating leakage of cytochrome c from mitochondria into the cytosol. We also found that the intensity of green light was proportional to both incubating time and concentration of oridonin. The combination of these observations suggested the release of cytochrome c from mitochondria to cytosol in response to treatment with oridonin, which might be the critical step in the process of oridonin-mediated apoptosis.

Structure–Activity Relationships Studies. Above experiments clarified that the loss of cancer cell viability was associated with the decreased mitochondrial membrane potential and the release of cytochrom c. Further studies were conducted to explore which unique pharmacophore of oridonin can initiate these biological responses. We compared the localization of probe **17d** when preincubated with oridonin (**1**), its 14-OH modified derivative (**25**), and α,β-unsaturated ketone reduction product (**26**), respectively. When A549 cells were pretreated with oridonin or its analogues, both **1** and **25** could block the uptake of probe **17d** effectively as shown in Figure 8a,b. However, no significant changes in both fluorescence intensity and localization of **17d** were noted when A549 cells were pretreated with 20 μM **26** for 24 h. This observation suggests that oridonin and its fluorescent probes act similarly in A549 cell and probe **17d** might share a common target with oridonin or its derivative **25**. More importantly, the active α,β-unsaturated ketone could bind tightly to the target in an irreversible manner.[43,44] Indeed, α,β-unsaturated ketone moiety is a common and structurally important functionality that is widespread in various naturally occurring products, especially in *ent*-kaurane diterpenoids.[45,46] As shown in Figure

DOI: 10.1021/acs.jmedchem.6b00408
J. Med. Chem. 2016, 59, 5022−5034

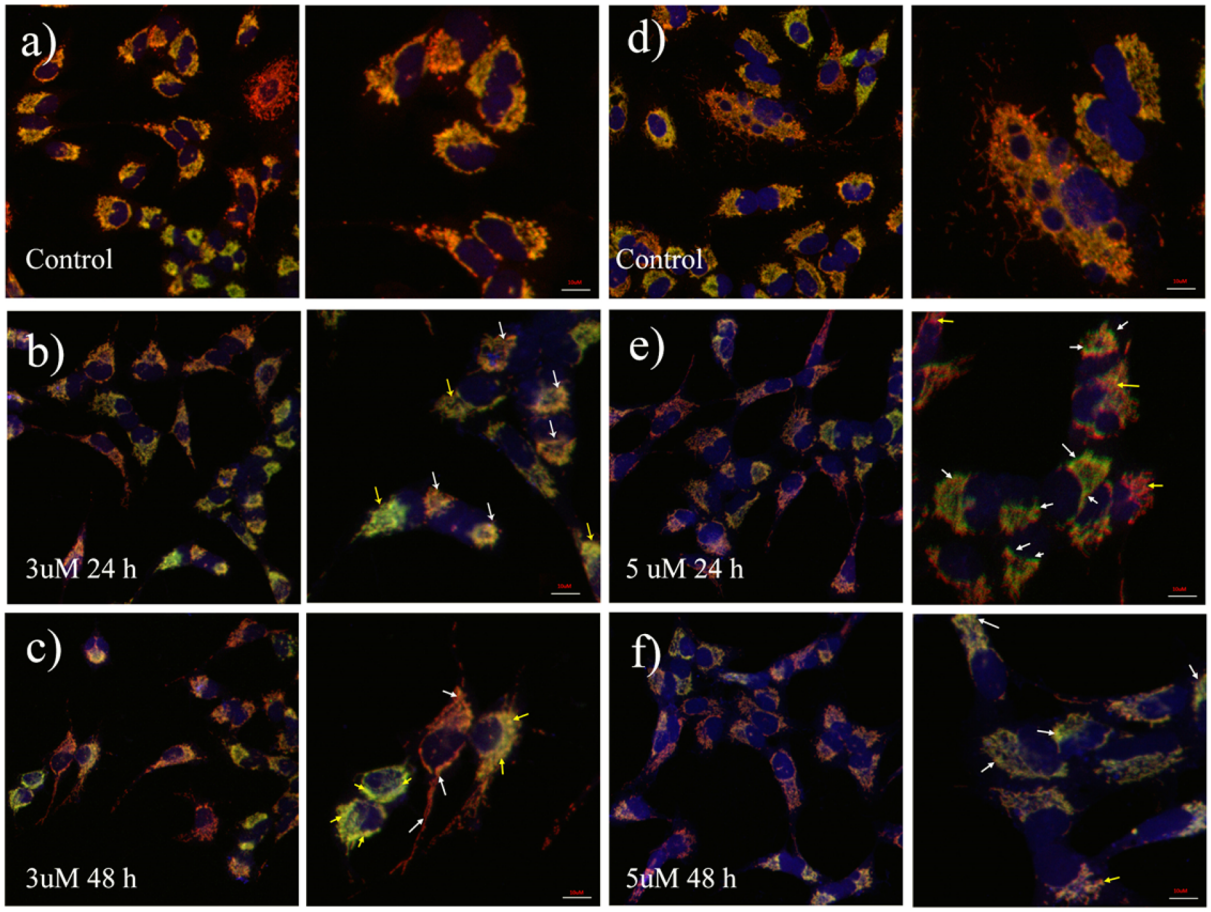

Figure 7. Immunofluorescence co-localization analysis reveals the release of cytochrome c from mitochondrion to cytosol during the apoptostic process. Cells were incubated with primary antibody against cytochrome c followed by treatment with Alexa Fluor 488-conjugated (green) goat antirabbit secondary antibody. The mitochondria were stained with Mitotracker Red (red), and cell nuclei were stained with DAPI (blue). Images were collected using confocal microscopy (LSM710 NLO, Zeiss). (a) A549 cells incubated without oridonin, right panel; merged images, left panel; enlarged view of representative cells. (b) A549 cells incubated with 3 μM **1** for 24 h, 48 h; (c) 5 μM **1** for 24 h (d), 48 h (e). Yellow arrow, cytochrome c located in mitochondria; white arrow, cytochrome c released from mitochondria to cytosol. Bars denote 10 μm.

1, almost all the *ent*-kaurane diterpenoids that exhibit substantial antitumor activity share this common moiety, and this result provides direct evidence that the *ent*-kaurane diterpenoids might share a common mode of action.

CONCLUSION

In this experiment, nine novel fluorescent analogues were designed and synthesized to visualize the anticancer mechanism of action of oridonin. Most of the target probes displayed satisfactory antiproliferative activities and optimal fluorescent properties. Further fluorescent and biological profiles were examined by using typical probes (**17d**, **24a**, and **27**) to investigate the mode of action of oridonin in cancer cell lines. It was demonstrated that oridonin fluorescent probe **17d** could be absorbed quickly by cancer cells, and α,β-unsaturated ketone moiety was the key pharmacophore for the anticancer activity and uptake of oridonin. Moreover, time-based subcellular localization studies of probe **17d** in A549 cells were performed, and the co-localization analysis illustrated the mitochondria-specific localization of fluorescent oridonin probe **17d**, which could be developed as a specific mitochondria biomarker. The subsequent studies on mitochondrial physiology indicated that the mitochondrial pathway is involved in oridonin-mediated apoptosis and that cytochrome c plays an important role in the apoptotic process.

In summary, we report an effective strategy for fluorescent labeling of oridonin, which may be used for studies on other *ent*-kaurane diterpenoids for which the anticancer action and targets are currently unknown. Further progress on identification of cellular targets of oridonin and other *ent*-kaurane diterpenoids will be reported in due course.

EXPERIMENTAL SECTION

Chemistry. *General Information.* Commercially available reagents and solvents were used without further purification. Column chromatography was carried out on Merck silica gel 60 (200−400 mesh). ^{1}H, ^{13}C, and 2D NMR spectra were recorded with 300 MHz spectrometers in the indicated solvents (TMS as internal standard). Chemical shifts were reported in parts per million (ppm, δ) downfield from tetramethylsilane. Proton coupling patterns are described as singlet (s), doublet (d), triplet (t), quartet (q), double doublet (dd), multipet (m), and broad (br). Low- and high-resolution mass spectra (LRMS and HRMS) were measured on Agilent QTOF 6520. Melting points were taken on XT-4 micro melting point apparatus and uncorrected. The purity of all tested compounds was characterized by HPLC analysis, and individual compounds with a purity of ≥95% were used for subsequent experiments (see the Supporting Information). HPLC was performed using Phenomenex Gemini C18 (4.6 mm× 150 mm, 5 μm), and samples were detected using a wavelength of 240 nm.

DOI: 10.1021/acs.jmedchem.6b00408
J. Med. Chem. 2016, 59, 5022−5034

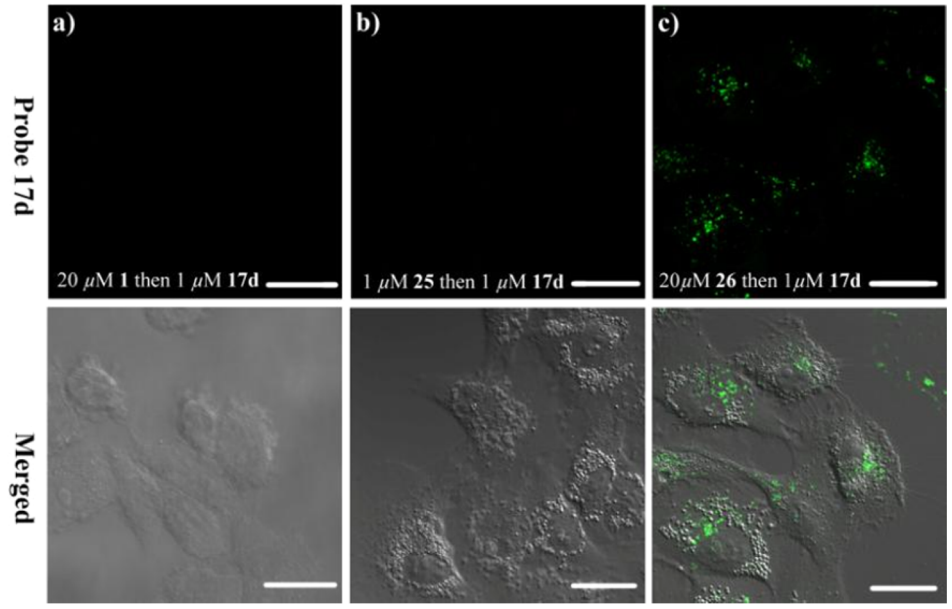

Figure 8. Confocal fluorescent images detailing the impact of compounds **1**, **25**, and **26** on the subcellular localization of probe **17d**. A549 cells were incubated with 20 μM oridonin (**1**) (a), 1 μM **25** (b), 20 μM **26** (c) for 24 h, then 1 μM probe **17d** for 1 h. Images were collected with excitation of probe at λ_{ex} = 405 nm and emission at λ_{em} = 460 nm, cells were imaged at 40× with an inverted confocal microscope (LSM710 NLO, Zeiss). DIC: differential interference contrast field. Bars denote 10 μm.

*^{1}H NMR and ^{13}C NMR Spectra of the Representive Compounds and Probes. Synthesis of Probe **17d**.* Compound **1** (100 mg, 0.27 mmol) was dissolved in dichloromethane, then EDCI, DMAP, and coumarin intermediates **16d** (120 mg, 0.27 mmol) were added. The reaction mixture was stirred at room temperature for 1 h. Then the mixture was washed with 10% HCl. The organic layer was washed with brine and dried over anhydrous Na_2SO_4. After flash chromatography (dichloromethane/methanol 150:1), compound **17d** was obtained as a yellow solid (171 mg, 80%); mp 130−131 °C. ^{1}H NMR($CDCl_3$, 300 MHz), δ (ppm) 8.42 (1H, s), 7.37 (1H, d, J = 8.94 Hz), 6.62 (1H, dd, J = 8.97, 2.34 Hz), 6.46 (1H, d, J = 2.16 Hz), 6.05 (1H, s), 6.07 (1H, d, J = 10.50 Hz), 5.88 (1H, s), 5.51 (1H, s), 4.20−4.34 (3H, m, 20-CH_2), 4.05−4.15 (4H, m), 3.73 (1H, m), 3.42−3.52 (5H, m), 3.17 (1H, d, J = 9.81 Hz), 2.60 (1H, m), 2.29−2.37 (4H, m), 2.29 (1H, m), 1.97 (1H, m), 1.90 (2H, m), 1.85−1.95 (4H, m), 1.73 (1H, m), 1.68 (1H, m), 1.58 (1H, m), 1.44 (1H, m), 1.30 (1H, m), 1.21−1.24 (2H, m), 1.24 (6H, t, J = 7.14 Hz), 1.88 (6H, s). ^{13}C NMR($CDCl_3$, 75 MHz), δ (ppm) 206.5, 172.7, 171.3, 164.2, 158.4, 158.2, 152.9, 149.9, 149.2, 131.1, 120.0, 109.5, 108.8, 107.7, 96.7, 96.1, 76.4, 74.1, 73.4, 64.5, 64.0, 63.4, 61.9, 59.7, 54.6, 45.0, 41.3, 38.7, 33.7, 33.5, 33.0, 32.5, 30.5, 30.0, 29.6, 25.4, 25.3, 21.6, 19.8, 19.8, 12.4. MS (ESI) m/z: 792.4 $[M - H]^-$, 794.6 $[M + H]^+$. HR-MS (ESI) m/z: calcd for $C_{43}H_{56}NO_{13}$ $[M + H]^+$ 794.3746, found 794.3765.

*Synthesis of Probe **24a**.* Following the procedure described for the preparation of compound **17d**, compound **24a** was synthesized as a pale-yellow solid (yield 73%); mp 147−148 °C. ^{1}H NMR ($CDCl_3$, 300 MHz): δ (ppm) 1.09 (s, 3H), 1.11 (s, 3H), 1.26 (m, 4H), 1.61 (m, 7H), 1.97 (m, 1H), 2.22 (m, 1H), 2.57 (m, 4H), 3.07 (s, 6H, $N(CH_3)_2$), 3.15 (m, 1H), 3.50 (m, 1H), 3.74 (s, 2H), 4.05 (d, J = 8.7 Hz, 1H), 4.28 (m, 5H), 5.52 (s, 1H), 5.90 (s, 1H), 6.04 (m, 1H), 6.09 (s, 1H), 6.15 (s, 1H, Ar-H), 6.57 (s, 1H, Ar-H), 6.66 (d, J = 9.0 Hz, 1H, Ar-H), 7.43 (d, J = 9.0 Hz, 1H, Ar-H). ^{13}C NMR ($CDCl_3$, 75 MHz): δ (ppm) 206.0, 171.3, 170.3, 168.5, 161.3, 155.4, 152.5, 149.4, 147.7, 124.8, 119.7, 110.2, 108.6, 107.9, 97.8, 95.6, 75.7, 73.8, 72.9, 62.8, 62.5, 61.7, 61.5, 59.0, 54.2, 40.8, 39.6, 38.2, 37.3, 33.2, 32.1, 30.0, 29.8, 29.4, 29.1, 21.2, 19.3. MS (ESI) m/z: 736.3 $[M - H]^-$, 738.5 $[M + H]^+$. HR-MS (ESI) m/z: calcd for $C_{39}H_{48}NO_{13}$ $[M + H]^+$ 738.3129, found 738.3131.

*Synthesis of Compound **25**.* Compound **1** (200 mg, 0.55 mmol) was dissolved in dichloromethane, then EDCI, DMAP and *n*-caprylic acid (79 mg, 0.55 mmol) were added. The reaction mixture was stirred at room temperature for 2 h. Then the mixture was washed with 10% HCl. The organic layer was washed with brine and dried over anhydrous Na_2SO_4. After flash chromatography (dichloromethane/methanol 200:1), compound **25** was obtained as a white solid (216 mg, 80%); mp 69−71 °C. ^{1}H NMR ($CDCl_3$, 300 MHz): δ (ppm) 6.24 (d, J = 9.4 Hz, 1H), 6.13 (s, 1H), 5.81 (s, 1H), 5.48 (s, 1H), 4.37 (s, 1H), 3.30, 4.07 (dd, $J_A = J_B$ = 9.6 Hz, each 1H), 3.75 (m, 1H), 3.50 (m, 1H), 3.18 (d, J = 9.6 Hz, 1H), 2.62 (m, 1H), 2.27 (m, 3H), 2.01 (m, 1H), 1.54 (m, 8H), 1.24 (m, 10H), 1.10 (s, 6H), 0.82 (m, 3H). ^{13}C NMR ($CDCl_3$, 75 MHz): δ (ppm) 206.7, 172.1, 149.8, 120.0, 96.2, 76.7, 73.8, 73.1, 63.5, 61.8, 59.9, 54.6, 41.3, 41.2, 38.6, 34.5, 33.7, 32.5, 31.5, 30.5, 30.3, 29.8, 29.6, 24.8, 24.6, 22.5, 21.6, 13.8. MS (ESI) m/z: 491.3 $[M + H]^+$. HR-MS (ESI) m/z: calcd for $C_{28}H_{42}NaO_7$ $[M + Na]^+$ 513.2823, found 513.2841.

*Synthesis of Compound **26**.* Compound **1** (200 mg) was dissolved in methyl alcohol (10 mL), then 10% Pd/C 20 mg was added to this solution. The mixture was stirred under hydrogen atmosphere at room temperature for 1 h. The reaction mixture was filtered, and the solvent was evaporated under reduced pressure. Flash chromatography of the residue, eluting with dichloromethane−methanol (40:1), gave compound **26** (188 mg, 94%) as a white solid; mp 206−207 °C. ^{1}H NMR (DMSO-d_6, 300 MHz): δ (ppm) 0.96 (s, 3H), 0.99 (s, 3H), 1.03(d, J = 7.2 Hz, 3H), 1.06 (m, 1H), 1.19 (m, 2H), 1.29 (m, 1H), 1.47 (m, 4H), 1.62 (m, 1H), 1.88 (m, 1H), 2.00 (m, 1H), 2.32 (m, 1H), 2.91 (m, 1H), 3.43 (m, 1H), 4.06, 3.81 (dd, $J_A = J_B$ = 10.8 Hz, each 1H, 20-CH_2), 4.06 (d, J = 4.8 Hz, 1H), 4.79 (s, 1H), 5.73 (d, J = 11.1 Hz, 1H), 6.09 (s, 1H), 6.73 (s, 1H). ^{13}C NMR (DMSO-d_6, 75 MHz): δ (ppm) 224.6, 96.7, 96.5, 73.2, 73.0, 71.4, 62.7, 61.1, 60.2, 52.6, 44.7, 38.3, 38.2, 33.3, 32.4, 29.2, 21.4, 19.0, 18.2, 10.1. MS(ESI) m/z: 367.8 $[M + H]^+$. HR-MS (ESI) m/z: calcd for $C_{20}H_{30}NaO_6$ $[M + Na]^+$ 389.1935, found 389.1939. The β-orientation of 17-CH_3 has been confirmed by literature report.[47]

*Synthesis of Probe **27**.* Following the procedure described for the preparation of compound **17d**, compound **27** was synthesized as a yellow solid; (yield 82%); mp 126−127 °C. ^{1}H NMR ($CDCl_3$, 300 MHz): δ (ppm) 1.01 (s, 3H), 1.06 (m, 3H), 1.14 (s, 3H), 1.16 (t, J = 7.2 Hz, 6H, $N(CH_2\underline{CH_3})_2$), 1.52 (m, 7H), 1.85 (m, 5H), 1.90 (m, 4H), 2.21 (m, 1H), 2.34 (m, 4H), 2.58 (m, 1H), 2.78 (m, 1H), 3.41 (q, J = 7.2 Hz, 4H, $N(\underline{CH_2}CH_3)_2$), 3.60 (m, 1H), 4.19, 3.96 (dd, $J_A = J_B$ = 10.8 Hz, each 1H, 20-CH_2), 4.08 (m, 2H), 4.27 (m, 2H), 5.72 (d, J = 11.4 Hz, 1H), 5.90 (d, J = 1.2 Hz, 1H), 6.39 (d, J = 2.4 Hz, 1H,

DOI: 10.1021/acs.jmedchem.6b00408
J. Med. Chem. 2016, 59, 5022−5034

Ar−H), 6.54 (dd, J = 9.0, 2.4 Hz, 1H, Ar-H), 7.30 (d, J = 9.0 Hz, 1H, Ar-H), 8.35 (1H, s, Ar-H). ^{13}C NMR ($CDCl_3$, 75 MHz): δ (ppm) 221.9, 172.1, 170.7, 158.0, 152.5, 130.6, 125.0, 109.1, 107.2, 96.2, 95.4, 76.5, 73.8, 72.9, 64.1, 63.6, 63.0, 61.0, 60.2, 59.5, 54.0, 53.0, 45.6, 44.6, 40.5, 38.2, 38.0, 36.6, 33.2, 33.1, 32.6, 32.0, 31.7, 29.8, 29.2, 24.9, 24.8, 20.8, 19.3, 13.4, 11.9, 9.3. MS (ESI) m/z: 794.4 $[M - H]^-$, 796.6 $[M + H]^+$. HR-MS (ESI) m/z: calcd for $C_{43}H_{58}NO_{13}$ $[M + H]^+$ 796.3903, found 796.3907.

Cytotoxicity Assay. The effect of oridonin and its derivatives on the cytotoxicity of cancer cells was determined by MTT assay. Briefly, the MTT assay was performed in 96-well plates using HepG2, A549, and HeLa cells. These cells (5×10^4 cells/mL) at the log phase of their growth cycle were added to each well (100 μL/well), then treated in the presence or absence of test compounds and incubated for 72 h at 37 °C in a humidified atmosphere of 5% CO_2. After terminating the treatment, 20 μL of MTT solution (5 mg/mL) was added to each cultured medium and cells were incubated for another 4 h. Then, DMSO was added to each well (150 μL/well). After 10 min at room temperature, the OD value of each well was measured on a microplate reader (BIO-RAD Instruments Inc. no. 550) at the wavelength of 490 nm. In these experiments, the negative reference agent was 0.1% DMSO, and paclitaxel at the concentration of 10 mg/mL was used as the positive reference.

Fluorescent Cell Staining. For fluorescence observation, A549 cells were seeded in Lab-Tek four-chambered slides (Nalge Nunc International, Naperville, IL, USA) and incubated with various concentrations of fluorescent oridonin derivatives for different time. After incubation, cells were washed with PBS for three times and antifade mounting medium was added. Images were obtained with an inverted confocal microscope (LSM710 NLO, Zeiss). Each experiment was repeated three times, and selected images were presented in the manuscript.

Subcellular Localization Studies. A549 cells were seeded in Lab-Tek four-chambered slides (Nalge Nunc International, Naperville, IL, USA), pretreated with 1 μM **17d** for 1, 3, 12, 24 h, washed with PBS, and incubated with MitoTracker (Life Technologies Inc., USA, MitoTracker Red CMXRos, 200 nM) for another 0.5 h. After being washed with cold PBS, the cells were fixed with paraformaldehyde and washed before they were imaged with confocal laser scanning microscopy (LSM710 NLO, Zeiss).

JC-1 Assay to Determine MMP. The MMP was determined with the dual-emission mitochondrial dye JC-1. Cells were loaded with 10 μg/mL JC-1 dye for 30 min at 37 °C and then washed for 5 min in PBS buffer. After incubation, samples were immediately assessed for red and green fluorescence by a microplate reader. The fluorescent signal of monomers is measured with an excitation wavelength of 490 nm and an emission wavelength of 535 nm. The fluorescent signal of aggregates is detected with an excitation wavelength of 525 nm and an emission wavelength of 600 nm. Besides, the fluorescent signal can also be detected using confocal microscope. All the experiments were performed in triplicate.

Immunofluorescence Co-localization Analysis. A549 cells were grown on coverslips inside a Petri dish filled with the appropriate culture medium. When cells have reached the desired confluency, the media was removed from the dish and prewarmed (37 °C) staining solution containing MitoTracker probe was added. The cells were incubated for 30 min under growth conditions. After staining was complete, staining solution was replaced with washing buffer. After fixing with 4% formaldehyde and permeabilizing with 0.2% TritonX-100, cells were blocked with 5% BSA (Amresco) for 1 h at room temperature. Cells were incubated with primary antibody against cytochrome c (Biolegend) overnight at 4 °C, followed by incubated with Alexa Fluor 488-conjugated goat antirabbit secondary antibody (Molecular Probe, Grand Island, NY) for 2 h in room temperature. Nuclei were counter stained with DAPI. Cells were imaged with confocal laser scanning microscopy (LSM710 NLO, Zeiss). Fluorescence excitation and emission spectra for MitoTracker Red CMXRos are 579 and 599 nm and those for Alexa Fluor are 495 and 519 nm.

■ ASSOCIATED CONTENT

Supporting Information

The Supporting Information is available free of charge on the ACS Publications website at DOI: 10.1021/acs.jmedchem.6b00408.

NMR spectra of other snythesized compounds and copies of NMR spectra on the probes; 2D NMR of probe **17d**; HPLC analysis of tested compounds; stability test of probe **17d** in cells as well as cellular imaging studies (PDF)

Molecular formula strings (CSV)

■ AUTHOR INFORMATION

Corresponding Authors

*For J.Y.X.: phone, +86-25-83271299; fax, +86-25-83302827; E-mail, jinyixu@china.com.

*For F.W.: phone, +86-21-34207545; fax, +86-21-34207545; E-mail, fang.wu@sjtu.edu.cn.

Present Address

#For X.M.: Centre for Systems Chemistry, Stratingh Institute, University of Groningen, Nijenborgh 4, 9747 AG Groningen, The Netherlands.

Author Contributions

△S.X. and S.L. contributed equally.

Notes

The authors declare no competing financial interest.

■ ACKNOWLEDGMENTS

We thank COUP-US.com (New Jersey, USA) for editing of the article. This work is supported by the National Natural Science Foundation (no. 81373280), the Project Program of State Key Laboratory of Natural Medicines, China Pharmaceutical University (no. SKLNMZZCX201404), and China Postdoctoral Science Foundation (no. 2015M581903).

■ ABBREVIATIONS USED

MAPK, mitogen-activated protein kinase; CDK1, cyclin-dependent kinase; HSP70 1A, heat shock protein 70 1A; SAR, structure−activity relationship; EDCI, *N*-(3-(dimethylamino)propyl)-*N*′-ethylcarbodiimide hydrochloride; DMAP, *p*-*N*,*N*-dimethylaminopyridine; MTT, 3-(4,5-dimethylthiazol-2-yl)-2,5-diphenyltetrazolium bromide; MMP, mitochondrial membrane potential; JC-1, 5,5′,6,6′-tetrachloro-1,1′,3,3′-tetraethyl-imidacarbocyanine iodide

■ REFERENCES

(1) Khazir, J.; Riley, D. L.; Pilcher, L. A.; De-Maayer, P.; Mir, B. A. Anticancer agents from diverse natural sources. *Nat. Prod. Commun.* **2014**, *9*, 1655−1669.

(2) Butler, M. S.; Robertson, A. A.; Cooper, M. A. Natural product and natural product derived drugs in clinical trials. *Nat. Prod. Rep.* **2014**, *31*, 1612−1661.

(3) Sun, H. D.; Huang, S. X.; Han, Q. B. Diterpenoids from *Isodon* species and their biological activities. *Nat. Prod. Rep.* **2006**, *23*, 673−698.

(4) Chen, S.; Gao, J.; Halicka, H. D.; Huang, X.; Traganos, F.; Darzynkiewicz, Z. The cytostatic and cytotoxic effects of oridonin (Rubescenin), a diterpenoid from Rabdosia rubescens, on tumor cells of different lineage. *Int. J. Oncol.* **2005**, *26*, 579−588.

(5) Zhao, Y.; Niu, X. M.; Qian, L. P.; Liu, Z. Y.; Zhao, Q. S.; Sun, H. D. Synthesis and cytotoxicity of some new eriocalyxin B derivatives. *Eur. J. Med. Chem.* **2007**, *42*, 494−502.

DOI: 10.1021/acs.jmedchem.6b00408
J. Med. Chem. 2016, 59, 5022−5034

(6) Zou, Q. F.; Du, J. K.; Zhang, H.; Wang, H. B.; Hu, Z. D.; Chen, S. P.; Du, Y.; Li, M. Z.; Xie, D.; Zou, J.; Sun, H. D.; Pu, J. X.; Zeng, M. S. Anti-tumor activity of longikaurin A (LK-A), a novel natural diterpenoid, in nasopharyngeal carcinoma. *J. Transl. Med.* **2013**, *11*, 200−210.
(7) Jiang, H. Y.; Wang, W. G.; Zhou, M.; Wu, H. Y.; Zhan, R.; Li, X. N.; Du, X.; Li, Y.; Pu, J. X.; Sun, H. D. Enmein-type 6,7-*seco*-*ent*-kauranoids from *Isodon* sculponeatus. *J. Nat. Prod.* **2013**, *76*, 2113−2119.
(8) Han, Q. B.; Li, M. L.; Li, S. H.; Mou, Y. K.; Lin, Z. W.; Sun, H. D. *Ent*-kaurane diterpenoids from *Isodon rubescens* var. *lushanensis*. *Chem. Pharm. Bull.* **2003**, *51*, 790−793.
(9) Lin, Z. M.; Guo, Y. X.; Gao, Y. H.; Wang, S. Q.; Wang, X. N.; Xie, Z. Y.; Niu, H. M.; Chang, W. Q.; Liu, L.; Yuan, H. Q.; Lou, H. X. *ent*-Kaurane diterpenoids from Chinese liverworts and their antitumor activities through michael addition as detected in situ by a fluorescence probe. *J. Med. Chem.* **2015**, *58*, 3944−3956.
(10) Ding, C. Y.; Zhang, Y. S.; Chen, H. J.; Yang, Z. D.; Wild, C.; Ye, N.; Ester, C. D.; Xiong, A. L.; White, M. A.; Shen, Q.; Zhou, J. Oridonin ring A-based diverse constructions of enone functionality: identification of novel dienone analogues effective for highly aggressive breast cancer by inducing apoptosis. *J. Med. Chem.* **2013**, *56*, 8814−8825.
(11) Ding, C. Y.; Zhang, Y. S.; Chen, H. J.; Yang, Z. D.; Wild, C.; Chu, L. L.; Liu, H. L.; Shen, Q.; Zhou, J. Novel nitrogen-enriched oridonin analogues with thiazole-fused A-ring: protecting group-free synthesis, enhanced anticancer profile, and improved aqueous solubility. *J. Med. Chem.* **2013**, *56*, 5048−5058.
(12) Ding, C. Y.; Wang, L. L.; Chen, H. J.; Wild, C.; Ye, N.; Ding, Y.; Wang, T. Z.; White, M. A.; Shen, Q.; Zhou, J. *ent*-Kaurane-based regio- and stereoselective inverse electron demand hetero-Diels-Alder reactions: synthesis of dihydropyran-fused diterpenoids. *Org. Biomol. Chem.* **2014**, *12*, 8442−8452.
(13) Xu, S. T.; Pei, L. L.; Wang, C. Q.; Zhang, Y. K.; Li, D. H.; Yao, H. Q.; Wu, X. M.; Chen, Z. S.; Sun, Y. J.; Xu, J. Y. Novel hybrids of natural oridonin-bearing nitrogen mustards as potential anticancer drug candidates. *ACS Med. Chem. Lett.* **2014**, *5*, 797−802.
(14) Owona, B. A.; Schluesener, H. J. Molecular insight in the multifunctional effects of oridonin. *Drugs R&D* **2015**, *15*, 233−244.
(15) Li, C. Y.; Wang, E. Q.; Cheng, Y.; Bao, J. K. Oridonin, An active diterpenoid targeting cell cycle arrest, apoptotic and autophagic pathways for cancer therapeutics. *Int. J. Biochem. Cell Biol.* **2011**, *43*, 701−704.
(16) Liu, Y.; Liu, Y. Z.; Zhang, R. X.; Wang, X.; Meng, Z. J.; Huang, J.; Wu, K.; Luo, J. Y.; Zuo, G. W.; Chen, L.; Yin, L. J.; Deng, Z. L.; He, B. C. Oridonin inhibits the proliferation of human osteosarcoma cells by suppressing Wnt/beta-catenin signaling. *Int. J. Oncol.* **2014**, *45*, 795−803.
(17) Dong, Y. M.; Zhang, T.; Li, J. J.; Deng, H. Y.; Song, Y. J.; Zhai, D.; Peng, Y.; Lu, X. L.; Liu, M. Y.; Zhao, Y. X.; Yi, Z. F. Oridonin inhibits tumor growth and metastasis through anti-angiogensis by blocking the Notch signaling. *PLoS One* **2014**, *9*, e113830.
(18) Bu, H. Q.; Liu, D. L.; Wei, W. T.; Chen, L.; Huang, H.; Li, Y.; Cui, J. H. Oridonin induces apoptosis in SW1990 pancreatic cancer cells via p53- and caspase-dependent induction of p38 MAPK. *Oncol. Rep.* **2014**, *31*, 975−982.
(19) Xu, B.; Shen, W.; Liu, X.; Zhang, T.; Ren, J.; Fan, Y. J.; Xu, J. Oridonin inhibits BxPC-3 cell growth through cell apoptosis. *Acta Biochim. Biophys. Sin.* **2015**, *47*, 164−173.
(20) Dal Piaz, F.; Cotugno, R.; Lepore, L.; Vassallo, A.; Malafronte, N.; Lauro, G.; Bifulco, G.; Belisario, M. A.; De Tommasi, N. Chemical proteomics reveals HSP70 1A as a target for the anticancer diterpene oridonin in Jurkat cells. *J. Proteomics* **2013**, *82*, 14−26.
(21) Li, J.; Cisar, J. S.; Zhou, C. Y.; Vera, B.; Williams, H.; Rodríguez, A. D.; Cravatt, B. F.; Romo, D. Simultaneous structure-activity studies and arming of natural products by C-H amination reveal cellular targets of eupalmerin acetate. *Nat. Chem.* **2013**, *5*, 510−517.
(22) Robles, O.; Romo, D. Chemo- and site-selective derivatizations of natural products enabling biological studies. *Nat. Prod. Rep.* **2014**, *31*, 318−334.
(23) Böttcher, T.; Pitscheider, M.; Sieber, S. A. Natural products and their biological targets: proteomic and metabolomic labeling strategies. *Angew. Chem., Int. Ed.* **2010**, *49*, 2680−2698.
(24) Ziegler, S.; Pries, V.; Hedberg, C.; Waldmann, H. Target identification for small bioactive molecules: finding the needle in the haystack. *Angew. Chem., Int. Ed.* **2013**, *52*, 2744−2792.
(25) Terai, T.; Nagano, T. Small-molecule fluorophores and fluorescent probes for bioimaging. *Pfluegers Arch.* **2013**, *465*, 347−359.
(26) Yun, S. W.; Kang, N. Y.; Park, S. J.; Ha, H. H.; Kim, Y. K.; Lee, J. S.; Chang, Y. T. Diversity oriented fluorescence library approach (DOFLA) for live cell imaging probe development. *Acc. Chem. Res.* **2014**, *47*, 1277−1286.
(27) DeGuire, S. M.; Earl, D. C.; Du, Y.; Crews, B. A.; Jacobs, A. T.; Ustione, A.; Daniel, C.; Chong, K. M.; Marnett, L. J.; Piston, D. W.; Bachmann, B. O.; Sulikowski, G. A. Fluorescent probes of the apoptolidins and their utility in cellular localization studies. *Angew. Chem., Int. Ed.* **2015**, *54*, 961−964.
(28) Li, C.; Dong, T.; Li, Q.; Lei, X. G. Probing the anticancer mechanism of (−)-ainsliatrimer A through diverted total synthesis and bioorthogonal ligation. *Angew. Chem., Int. Ed.* **2014**, *53*, 12111−12115.
(29) Jurášek, M.; Rimpelová, S.; Kmoníčková, E.; Drašar, P.; Ruml, T. Tailor-made fluorescent trilobolide to study its biological relevance. *J. Med. Chem.* **2014**, *57*, 7947−7954.
(30) Hughes, C. C.; MacMillan, J. B.; Gaudêncio, S. P.; Fenical, W.; La Clair, J. J. Ammosamides A and B target myosin. *Angew. Chem., Int. Ed.* **2009**, *48*, 728−732.
(31) Liu, Y. G.; Lok, C. N.; Ko, B. C.; Shum, T. Y.; Wong, M. K.; Che, C. M. Subcellular localization of a fluorescent artemisinin derivative to endoplasmic reticulum. *Org. Lett.* **2010**, *12*, 1420−1423.
(32) Wu, J.; Shen, Q.; Wang, Y.; Zhao, D.; Peng, C.; Li, J. X. Fluorescent probes for subcellular localization during osteclast formation. *ACS Med. Chem. Lett.* **2014**, *5*, 911−914.
(33) Kumar, K. A.; La Clair, J. J.; Fuchs, P. L. Synthesis and evaluation of a fluorescent ritterazine-cephalostatin hybrid. *Org. Lett.* **2011**, *13*, 5334−5337.
(34) Hughes, C. C.; Yang, Y. L.; Liu, W. T.; Dorrestein, P. C.; La Clair, J. J.; Fenical, W. Marinopyrrole A target elucidation by acyl dye transfer. *J. Am. Chem. Soc.* **2009**, *131*, 12094−12096.
(35) Xu, J. Y.; Yang, J. Y.; Ran, Q.; Wang, L.; Liu, J.; Wang, Z. X.; Wu, X. M.; Hua, W. Y.; Yuan, S. T.; Zhang, L. Y.; Shen, M. Q.; Ding, Y. F. Synthesis and biological evaluation of novel 1-*O*- and 14-*O*-derivatives of oridonin as potential anticancer drug candidates. *Bioorg. Med. Chem. Lett.* **2008**, *18*, 4741−4744.
(36) Hori, Y.; Norinobu, T.; Sato, M.; Arita, K.; Shirakawa, M.; Kikuchi, K. Development of fluorogenic probes for quick no-wash live-cell imaging of intracellular proteins. *J. Am. Chem. Soc.* **2013**, *135*, 12360−12365.
(37) Rong, L.; Liu, L. H.; Chen, S.; Cheng, H.; Chen, C. S.; Li, Z. Y.; Qin, S. Y.; Zhang, X. Z. A coumarin derivative as a fluorogenic glycoproteomic probe for biological imaging. *Chem. Commun.* **2014**, *50*, 667−669.
(38) Nagao, Y.; Fujita, E.; Kohno, T.; Yagi, M. An efficient method for selective acetylation of alcoholic hydroxyl groups. *Chem. Pharm. Bull.* **1981**, *29*, 3202−3207.
(39) Sinha, K.; Das, J.; Pal, P. B.; Sil, P. C. Oxidative stress: the mitochondria-dependent and mitochondria-independent pathways of apoptosis. *Arch. Toxicol.* **2013**, *87*, 1157−1180.
(40) Green, D. R.; Reed, J. C. Mitochondria and apoptosis. *Science* **1998**, *281*, 1309−1312.
(41) Yin, B.; Sheng, H.; Lin, J.; Zhou, H.; Zhang, N. The cell death of C6 astrocytoma cells induced by oridonin and its mechanism. *Int. J. Clin. Exp. Pathol.* **2012**, *5*, 562−568.
(42) Du, C. Y.; Fang, M.; Li, Y. C.; Li, L.; Wang, X. D. Smac, a mitochondrial protein that promotes cytochrome c-dependent caspase activation by eliminating IAP inhibition. *Cell* **2000**, *102*, 33−42.

DOI: 10.1021/acs.jmedchem.6b00408
J. Med. Chem. 2016, 59, 5022−5034

(43) Groll, M.; Schellenberg, B.; Bachmann, A. S.; Archer, C. R.; Huber, R.; Powell, T. K.; Lindow, S.; Kaiser, M.; Dudler, R. A plant pathogen virulence factor inhibits the eukaryotic proteasome by a novel mechanism. *Nature* **2008**, *452*, 755−758.
(44) Singh, J.; Petter, R. C.; Baillie, T. A.; Whitty, A. The resurgence of covalent drugs. *Nat. Rev. Drug Discovery* **2011**, *10*, 307−317.
(45) Festa, C.; Lauro, G.; De Marino, S.; D'Auria, M. V.; Monti, M. C.; Casapullo, A.; D'Amore, C.; Renga, B.; Mencarelli, A.; Petek, S.; Bifulco, G.; Fiorucci, S.; Zampella, A. Plakilactones from the marine sponge Plakinastrella mamillaris. Discovery of a new class of marine ligands of peroxisome proliferator-activated receptor γ. *J. Med. Chem.* **2012**, *55*, 8303−8317.
(46) Liu, C. X.; Yin, Q. Q.; Zhou, H. C.; Wu, Y. L.; Pu, J. X.; Xia, L.; Liu, W.; Huang, X.; Jiang, T.; Wu, M. X.; He, L. C.; Zhao, Y. X.; Wang, X. L.; Xiao, W. L.; Chen, H. Z.; Zhao, Q.; Zhou, A. W.; Wang, L. S.; Sun, H. D.; Chen, G. Q. Adenanthin targets peroxiredoxin I and II to induce differentiation of leukemic cells. *Nat. Chem. Biol.* **2012**, *8*, 486−493.
(47) Zhao, Y.; Niu, X. M.; Qian, L. P.; Liu, Z. Y.; Zhao, Q. S.; Sun, H. D. Synthesis and cytotoxicity of some new eriocalyxin B derivatives. *Eur. J. Med. Chem.* **2007**, *42*, 494−502.

DOI: 10.1021/acs.jmedchem.6b00408
J. Med. Chem. 2016, 59, 5022−5034